Electronic band structure of the $(GaAs)_1/(InAs)_1$ (111) superlattice

Rita Magri
Department of Physics, University of Modena, via Campi 213/A, I-41100 Modena, Italy
(Received 20 July 1989)

We present a first-principles calculation of the electronic band structure of $(GaAs)_1/(InAs)_1$ (111) superlattice, performed by using *ab initio* norm-conserving pseudopotentials. The folding in the smaller Brillouin zone and the new symmetry properties of the electronic states have been thoroughly investigated by a comparison with the band structure of the corresponding disordered alloy treated within the virtual-crystal approximation. The interactions between the folded states giving rise to energy splittings and electronic charge localization on given layers have been analyzed at the high-symmetry points. The effects of the new ordering potential, introduced by differentiating the two cations in the virtual crystal, and of the strain potential—arising when the superlattice is subjected to a lateral strain on the (111) planes—are separately investigated. We find a strong charge localization in the first two conduction states at the Γ point and a considerable minimum-band-gap reduction in the new ordered structure with respect to the virtual crystal. The strength of this localization and the fundamental band gap depend on the superlattice orientation and on the strain condition.

I. INTRODUCTION

Remarkable recent developments in materials growth techniques have made it possible to obtain ultrathin superlattices.[1-10] Moreover, a long-range order has been recently demonstrated to occur in ternary compounds of III-V semiconductors, such as $GaInAs_2$ or $GaInP_2$, grown by the vapor-levitation-epitaxy (VLE) technique.[8-10] In this case the order corresponds approximately to a monolayer (111) superlattice.

Considerable theoretical work has been recently devoted to gain insight into the structural and electronic properties of these new ordered systems. Among them, recent first-principles total-energy calculations on ultrathin superlattices have shown that these superstructures are generally unstable with respect to disproportionation into their zinc-blende-structure constituents.[11-19] This is due, for lattice-mismatched systems, mainly to the inability to minimize the positive microscopic strain by accommodating simultaneously in the same lattice distinct bond distance and bond angles nearest to those of the binary compounds. For lattice-matched superlattices, on the other hand, the instability is related to the charge transfer caused by the cations electronegativity difference which gives a positive contribution to the formation energy.[11,13-16] In addition to this intrinsic bulk instability, the role of the substrate and of the interfacial strains on the formation energy has been investigated.[20-24]

While the electronic properties of lattice-matched and [001]-grown semiconductor superlattices have been studied in great detail by using both first-principles and empirical methods,[11,12,25-29] there is not a comparable amount of information about the electronic band structure of [111] monolayer superlattices. Theoretical calculations of the electronic band structure of [111] III-V monolayer superlattices,[30-32] including the important issue of the optical bowings for different oriented superlattices,[32] have been performed only recently.

In this work we present a detailed study of the electronic band structure of the lattice-mismatched $(GaAs)_1/(InAs)_1$ (111) superlattice, by using a first-principles self-consistent calculation within the Hohenberg-Kohn-Sham density-functional theory (DFT). Although DFT, in the local-density approximation (LDA), is known to underestimate the fundamental band gaps,[33,34] our purpose here is to investigate the qualitative trends and the new features coming out in the band structure on passing from the zinc-blende-structure compounds to the superlattice. Significant results may be obtained by using the LDA as it has been shown in the literature.[11,25-32] In particular, we investigated the new features related to the following.

(1) The new ordering potential, whose shape and periodicity is closely related to the atomic configuration of the cations on their sublattice. This study is accomplished by a comparison between the band structures of the ordered superlattice and of the corresponding disordered alloy, where the ternary alloy has been treated within the virtual-crystal approximation (VCA).[19] In this context the folding and the band-mixing effects raising on passing to the new ordered configuration are analyzed.

(2) The particular superlattice stacking direction by detailing the differences with the electronic states of the monolayer (001) $GaInAs_2$ superlattice.

(3) The structural relaxation originated from the relatively large lattice mismatch (about 7%) between the two constituents of the superlattice.

The analysis of the first two items is worthwhile also in light of the very different behavior in the optical and transport properties between [111]- and [001]-grown superlattices and between the ordered and disordered ternary systems, as detailed by both experimental and theoretical investigations.[5,10,35]

As far as the third point is concerned, first-principles

studies of the effects of the epitaxial constraint, which is included in our superlattice relaxation model, on the band structure are scarce and prevalently restricted to the tetragonal [001]-grown direction.[27–29]

In order to determine a relaxed atomic configuration for the (111) monolayer superlattice we performed a first-principles self-consistent total-energy calculation. The relaxation model adopted to minimize the total energy has been described in detail elsewhere.[19]

II. CRYSTAL STRUCTURE

The superlattice structure, in the ideal (unrelaxed) configuration where all atoms are located in the zinc-blende sites, is obtained starting from the zinc-blende–structure crystal by arranging the (111) planes following the sequence: Ga, As, In, As, Ga, As, etc. The unit cell is doubled with respect to the primitive zinc-blende one and the structure belongs to the space group C_{3v}^5, or $R3m$. The interesting point about this geometry is that there are two inequivalent arsenic atoms with a different chemical environment: As(1), coordinated with one gallium and three indium atoms, and As(2), coordinated with one indium and three gallium atoms. This fact gives rise to a characteristic asymmetry in the electronic valence charge-density distribution and in the bonding charge around these atoms.[19] Further information on the atomic arrangement and on the structural parameters appropriate to this geometry is given in Ref. 19.

The Brillouin zone (BZ) is shown in Fig. 1. It is obtained by folding the fcc Brillouin zone along the [111] direction, on the midway Λ direction in the point called Z in the figure. The BZ volume is half of the fcc one. The folding operation makes the fcc L points inequivalent: the two points along the [111] direction map onto the Γ point, while the other six Λ directions turn out to correspond to the $\Gamma-F$ directions in the new Brillouin zone.

In order to compare the superlattice and binary-compound band structures it is suitable to give the correspondence between the **k** points in the two Brillouin zones. Each **k** point in the superlattice Brillouin zone, whose coordinates are (k_x,k_y,k_z), corresponds to two fcc

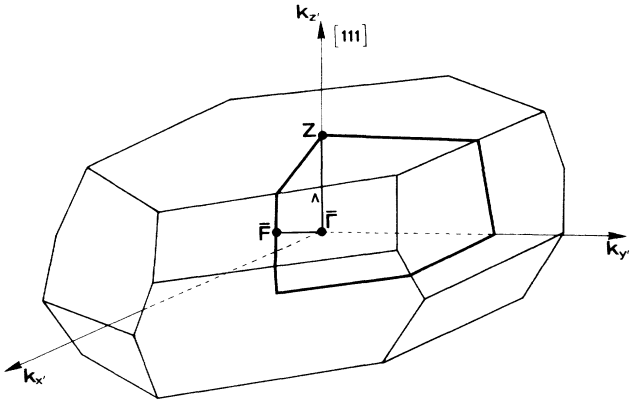

FIG. 1. The Brillouin zone for the $(GaAS)_1/(InAs)_1$ (111) superlattice referred to a rotated frame with the k_z axis along the [111] direction.

TABLE I. Character table for C_{3v} point group (Λ direction).

C_{3v} $(3m)$	E	$2C_3$	$3\sigma_d$
$\Lambda_1\bar{\Gamma}_1$	1	1	1
$\Lambda_2\bar{\Gamma}_2$	1	1	−1
$\Lambda_3\bar{\Gamma}_3$	2	−1	0

Brillouin-zone **k** points: (k_x,k_y,k_z) and $(\pm\frac{1}{2}-k_x,\pm\frac{1}{2}-k_y,\pm\frac{1}{2}-k_z)$, where the sign + (−) has to be taken by depending on whether the quantity $(1/\sqrt{3})k_x+(1/\sqrt{3})k_y+(1/\sqrt{3})k_z$ is positive (negative). Therefore, the correspondence relations at the high-symmetry points are the following (the superlattice BZ points are indicated by an overbar according to the notation introduced in Ref. 25):

$$\bar{\Gamma}\leftrightarrow\Gamma+L_{111}\ ,$$

$$\bar{F}\leftrightarrow X_{x,y,z}+L_{\bar{1}11,1\bar{1}1,11\bar{1}}\ .$$

To address the labels used for the superlattice electronic states to the appropriate irreducible representations we give the character tables for the Λ ($Z-\Gamma$) direction (Table I) and for the $\Gamma-F$ direction (Table II).[36]

III. ELECTRONIC BAND STRUCTURE OF $(GaAs)_1/(InAs)_1$ (111) SUPERLATTICE

The $(GaAs)_1/(InAs)_1$ (111) superlattice electronic band structure was calculated by using nonlocal norm-conserving pseudopotentials.[37] The single-particle wave functions were expanded in plane waves with energy of less than 14 Ry. To obtain the self-consistent total potential the calculation was performed by using a Ceperley-Adler form,[38] as parametrized by Perdew and Zunger,[39] for exchange and correlation effects and two special **k** points for the BZ integration. The calculation was iterated until the difference in the Fourier components of the potential between two subsequent iterations was less than 10^{-6} Ry. Further details can be found in Ref. 19. The 14-Ry cutoff ensures a convergence of about 0.1 eV on the Γ_{1c}-state energy in the binary compounds. Since we are interested in comparing corresponding band-energy differences for different systems, which are all treated in the same way, this convergence error, as well as the LDA error, should partially cancel.

We found the superlattice is a direct-gap material as the two binary constituents.

As for the total energy, it is usual to think the superlattice electronic band structure as having originated through three conceptual steps.[25,40]

TABLE II. Character table for C_{1h} point group ($\bar{\Gamma}-\bar{F}$ direction).

C_{1h} (m)	E	σ_d
$\bar{F}_1$	1	1
$\bar{F}_2$	1	−1

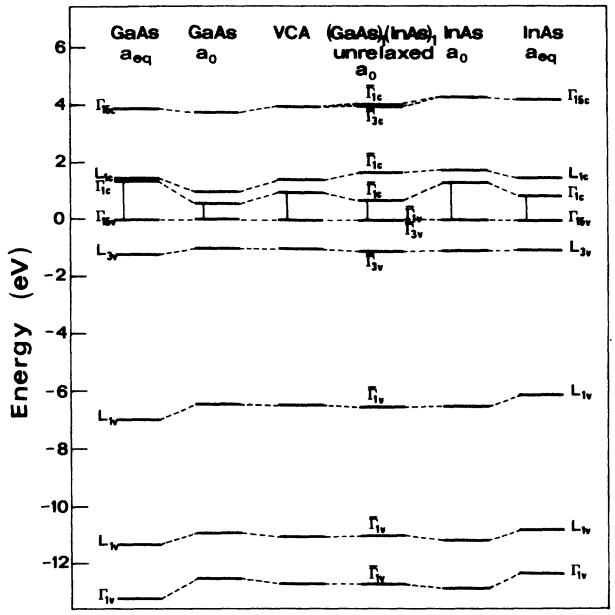

FIG. 2. Band eigenvalues at the Brillouin-zone center for cubic GaAs and InAs at their equilibrium lattice constants and at the common intermediate lattice constant $a_0=5.66$ Å, VCA $Ga_{0.5}In_{0.5}As$ disordered alloys, and unrelaxed $(GaAs)_1/(InAs)_1$ (111) superlattices. The cubic systems have been folded back into the half-volume Brillouin zone appropriate to a double unit cell.

A. From the binary compounds to the virtual crystal

The first contribution comes from the energy-band shifts that take place when InAs is compressed and GaAs is dilated from their equilibrium lattice constants to the intermediate unrelaxed superlattice one.[19] This contribution is usually called "volume deformation"[40] and includes the microscopic strain effects in the formation of the unrelaxed superlattice. The shifts are essentially induced by deformation-potential effects related to the uniform volume dilation or compression of the two binary systems. These shifts are generally such that for a uniform volume dilation the bonding-antibonding splitting between valence and conduction states diminishes. As a consequence, the fundamental band gap reduces. The relative band-energy shifts, with respect to the Γ_{15v} state, are depicted in Fig. 2.

The "intermediate" system, the virtual crystal, is then obtained by building a fictitious intermediate cation, whose atomic bare pseudopotential is given by the compositional average of the gallium and indium atomic bare pseudopotentials. The system so obtained can be considered intermediate between the two binary compounds, both with regard to the geometrical configuration [it is still a zinc-blende (ZB) compound with a lattice constant near the average value of the two parent binary compounds lattice constants] and with regard to the self-consistent ground-state valence-charge distribution, not substantially dissimilar from the average one.[19] The cation pseudopotential mixing effect upon the band structure is shown in Fig. 2, where the valence-band tops are aligned (a partial justification for this alignment is given below). We notice that the virtual-crystal electronic states are almost midway between the corresponding states of the two binary compounds, when they are considered at their equilibrium lattice constant or, equivalently, at the common intermediate lattice constant $a_0=5.66$ Å.

To give better evidence of the trends taking place on passing from the parent binary compounds to the virtual crystal, we compare in Table III the virtual-crystal electronic state energies with the averaged ones on the two parent binary compounds at their equilibrium lattice constants (first column) and at the lattice parameter, $a_0=5.66$ Å (second column), at the $\bar{\Gamma}$ point. Apart from the first two conduction bands in the virtual crystal, the trend is clear. The valence bands rise and the first two conduction bands lower, following approximately the

TABLE III. Calculated band eigenvalues at the $\bar{\Gamma}$ point relative to the valence-band maximum. The appropriate labels are used for the zinc-blende–structure and the corresponding superlattice states. Degeneracies are indicated in parentheses.

Level		$\bar{\varepsilon}=\frac{1}{2}\varepsilon_{GaAs,a_{eq}^{GaAs}}+\frac{1}{2}\varepsilon_{InAs,a_{eq}^{InAs}}$ (eV)	$\bar{\varepsilon}_0=\frac{1}{2}\varepsilon_{GaAs,a_0}+\frac{1}{2}\varepsilon_{InAs,a_0}$ (eV)	VCA (eV)	Unrelaxed superlattice (eV)	Relaxed superlattice (eV)
Valence bands						
$\Gamma_{1v}(1)$	$\bar{\Gamma}_{1v}(1)$	−12.762	−12.699	−12.654	−12.709	−12.728
$L_{1v}(1)$	$\bar{\Gamma}_{1v}(1)$	−11.065	−11.031	−11.003	−11.039	−11.111
$L_{1v}(1)$	$\bar{\Gamma}_{1v}(1)$	−6.553	−6.501	−6.442	−6.508	−6.599
$L_{3v}(2)$	$\bar{\Gamma}_{3v}(2)$	−1.114	−1.102	−1.095	−1.119	−1.224
$\Gamma_{15v}(3)$	$\bar{\Gamma}_{3v}(2)$	0.000	0.000	0.000	−0.006	0.000
	$\bar{\Gamma}_{1v}(1)$	0.000	0.000	0.000	0.000	−0.216
Conduction bands						
$\Gamma_{1c}(1)$	$\bar{\Gamma}_{1c}(1)$	1.129	0.952	1.055	0.701	0.456
$L_{1c}(1)$	$\bar{\Gamma}_{1c}(1)$	1.471	1.416	1.462	1.685	1.662
$\Gamma_{15c}(3)$	$\bar{\Gamma}_{3c}(2)$	4.050	4.053	4.057	3.965	3.831
	$\bar{\Gamma}_{1c}(1)$	4.050	4.053	4.057	4.013	3.851
$L_{3c}(2)$	$\bar{\Gamma}_{3c}(2)$	4.811	4.812	4.814	4.871	4.900

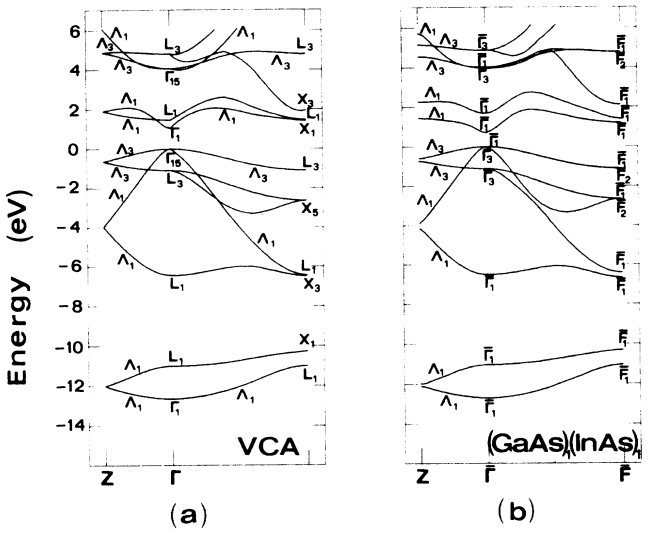

FIG. 3. Electronic band structures for (a) VCA disordered alloys and (b) unrelaxed $(GaAs)_1/(InAs)_1$ (111) superlattices.

trend in the lattice parameters $\frac{1}{2}(a_{eq}^{GaAs}+a_{eq}^{InAs})<a_0<a_{eq}^{VCA}$ (see Ref. 19). The highest conduction states are almost insensitive to the volume deformation (see also Fig. 2). The anomaly displayed by the first two virtual-crystal conduction states can be explained with the slightly larger polarity of this system with respect to the binary averaged system,[19] leading to the opening of the minimum band gap.

The virtual-crystal first conduction band in Γ (that is, the minimum band gap) is about 0.074 eV lower than the average gap value in the two parent binary compounds at their equilibrium volumes.

B. From the virtual crystal to the unrelaxed (111) monolayer superlattice

The next step is the introduction of the chemical disparity between the two cations. It has been found[12,18,19] that, relative to the two segregation products GaAs and InAs, the introduction of the two different cations on the appropriate crystal planes gives a small and positive contribution to the $GaInAs_2$ monolayer superlattice formation enthalpy. This contribution is related to a charge transfer between the crystal layers and to a charge rearrangement on the bonds.

Coming to the evolution of the band structure on passing from the virtual crystal to the superlattice, it is interesting to investigate the effects upon the band structure related to (a) the substitution of the virtual-crystal "average" cation with the two distinct ones on the appropriate crystal planes to obtain the new ordered structure with a lower symmetry, and (b) the particular superlattice orientation.

1. Passing from the disordered to the new ordered structure

With regard to the former point, in this work we limit ourselves to analyzing the new features revealed upon passing from the virtual crystal to a particular superstructure: the (111) monolayer superlattice. The changes in the band structure can be separated into two subsequent steps: the folding of the virtual-crystal energy bands into the superlattice Brillouin zone, due to the symmetry reduction, and the interaction between the folded bands, due to the new potential associated to the chemical difference between the two cations. The virtual-crystal folded bands are drawn in Fig. 3(a). They are labeled according to the nomenclature appropriate for the irreducible representations of the zinc-blende structure. Λ is the (111) superlattice longitudinal direction. The first VCA Λ_1 conduction band starts from the Γ_{1c} state, dispersing upwards initially. In Z it is folded back and disperses downward, then crosses the nonfolded part of the band, and finally gives rise to a new state in Γ (the folded state from the L point of the fcc Brillouin zone to Γ) at 1.462 eV, about 0.4 eV higher than the Γ_{1c} state. The difference between the calculated Γ_{1c} and L_{1c} states in the two binary systems is 0.02 eV in GaAs and

TABLE IV. The same as Table III for the band eigenvalues at the $\bar{F}$ point.

Level		VCA (eV)	Unrelaxed (eV)	Relaxed (eV)
Valence bands				
$L_{1v}(1)$	$\bar{F}_{1v}(1)$	−11.003	−11.040	−11.098
$X_{1v}(1)$	$\bar{F}_{1v}(1)$	−10.279	−10.304	−10.363
$X_{3v}(1)$	$\bar{F}_{1v}(1)$	−6.478	−6.670	−6.873
$L_{1v}(1)$	$\bar{F}_{1v}(1)$	−6.442	−6.401	−6.261
$X_{5v}(2)$	$\bar{F}_{2v}(1)$	−2.632	−2.655	−2.713
	$\bar{F}_{1v}(1)$	−2.632	−2.648	−2.772
$L_{3v}(2)$	$\bar{F}_{2v}(1)$	−1.095	−1.115	−1.125
	$\bar{F}_{1v}(1)$	−1.095	−1.102	−1.265
Conduction bands				
$X_{1c}(1)$	$\bar{F}_{1c}(1)$	1.405	1.400	1.271
$L_{1c}(1)$	$\bar{F}_{1c}(1)$	1.462	1.197	1.033
$X_{3c}(1)$	$\bar{F}_{1c}(1)$	1.943	2.112	1.962
$L_{3c}(2)$	$\bar{F}_{2c}(1)$	4.814	4.787	4.654
	$\bar{F}_{1c}(1)$	4.814	4.798	4.671

0.664 eV in InAs.

The introduction of the two cation pseudopotentials involves an interaction between the folded states with splittings and changes in their symmetry. The amount of the splitting is related to the intensity of the new coherent ordering potential, whose periodicity is doubled with respect to the virtual-crystal potential (it is possible to separate the superlattice self-consistent local potential into a virtual-crystal plus the new ordering components) and to its capability of coupling the folded zinc-blende states.[32] To analyze these splittings the unrelaxed superlattice band structure is drawn in Fig. 3(b), while the calculated band eigenvalues in the $\bar{\Gamma}$ and $\bar{F}$ points are given, respectively, in Tables III and IV, where the appropriate labels are used for both the zinc-blende and superlattice states. The Λ-direction symmetry does not change on passing from the virtual crystal to the superlattice and so the bands are fairly similar. The gap openings at the new zone boundary in Z, due to first-order effects of the ordering potential, are larger for the conduction than for the valence bands. The splitting of triply-degenerate Γ_{15} states into the two states $\bar{\Gamma}_1$ (nondegenerate) and $\bar{\Gamma}_3$ (doubly degenerate), due to the symmetry reduction, is only 0.006 eV for Γ_{15v} and 0.048 eV for Γ_{15c}. Moreover, the reduced symmetry prevents the two first conduction bands from crossing since they belong to the same irreducible representation. These bands split each other and the energy difference is 0.984 eV in the $\bar{\Gamma}$ point as compared to the corresponding value in the virtual crystal, 0.407 eV. This splitting is also in substantial agreement with that found in a linear augmented-plane-wave (LAPW) calculation on the lattice-matched $(GaAs)_1/(AlAs)_1$ (111) system.[32] As a consequence of this remarkable splitting, the minimum direct band gap reduces by 0.354 eV. This minimum-band-gap reduction in ordered superstructures is in agreement with the findings of other similar calculations[11,12,32] and accounts for some experimental results showing that this reduction takes place when ordering occurs in the corresponding ternary alloy.[5,10,41]

The electronic band coupling between the virtual-crystal folded bands can be analyzed by looking at the changes in the valence and conduction charge-density distributions that take place on passing from the virtual crystal to the superlattice. The virtual-crystal and superlattice charge-density distributions are compared in Figs. 4–6. In drawing these figures we have taken into account the correspondence between the virtual crystal and the superlattice states. The virtual crystal shares the same point group of the two binary compounds and, therefore, there are no changes in the composition and symmetry of its electronic states with respect to the binary systems.

We notice, first of all, that the initially equivalent virtual-crystal L points give rise to superlattice $\bar{\Gamma}$ and $\bar{F}$

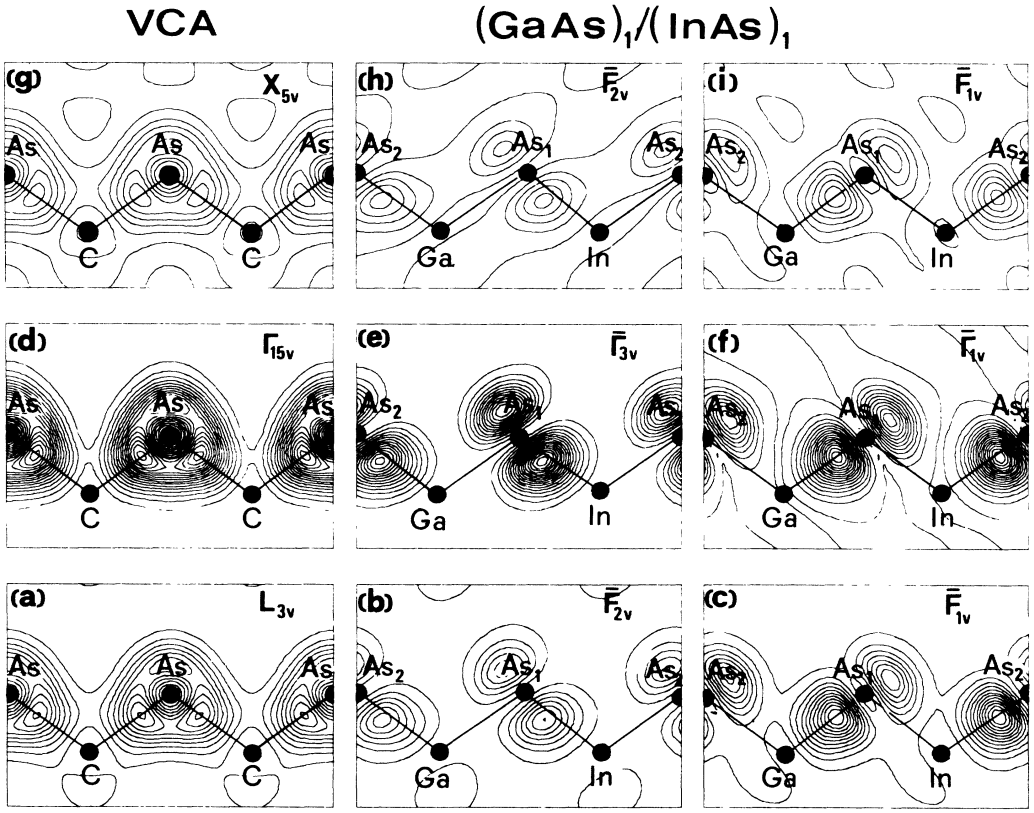

FIG. 4. Electronic charge density of high-symmetry valence states plotted in the $(1\bar{1}0)$ plane (one electron per volume $a_0^3/4$ at $a_0 = 5.66$ Å) for zinc-blende VCA alloys and unrelaxed $(GaAs)_1/(InAs)_1$ (111) superlattices. The step between the two neighboring contours is 1. [For convenience, As(1) and As(2) are sometimes equivalently represented as As_1 and As_2, respectively.]

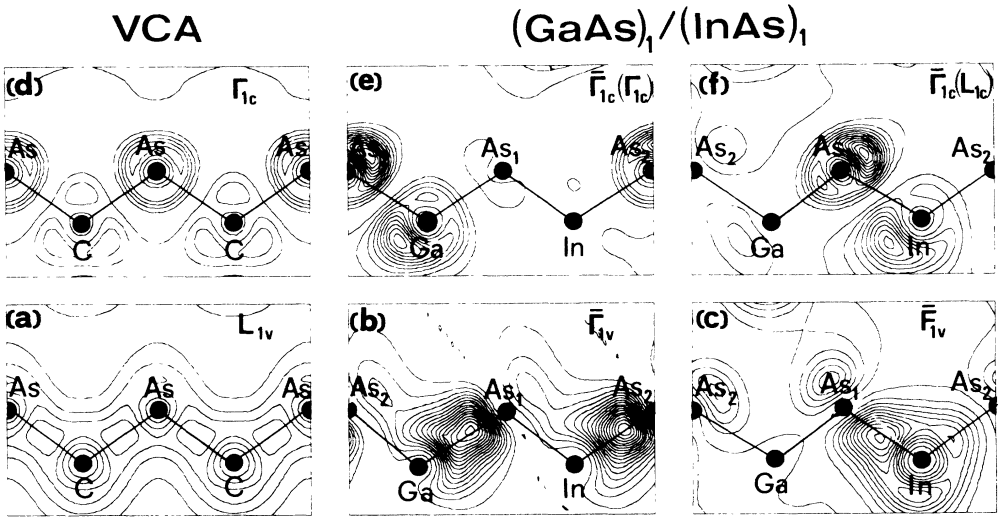

FIG. 5. The same as Fig. 4 for L_{1v}-, Γ_{1c}-, and L_{1c}-derived states. The step between two neighboring contours is 1 for the lowest plots and 2 for the uppermost plots.

states with different energies and a dissimilar charge-density distribution. Notice, for instance, from Figs. 5(a)–5(c), the two L_{1v}-derived states whose charge distributions show completely dissimilar features, related to the new symmetry properties of the **k** points.

The electronic charge-density distributions of the lowest valence states have not been plotted. In fact, the imposition of the superlattices' new long-range order has not a substantial effect upon them. These states of prevalently anionic s character lie approximately 11–12 eV below the valence-band maximum (VBM) and do not show substantial changes in the charge-density distribution, apart from a slight symmetry in the anionic bond charge related to the difference in the attractivity of the two cation pseudopotentials. Also, the interaction between these states is negligible as can be inferred by the observation that the band energies are more or less the same as in the virtual crystal [see Fig. 3(b) and Tables III and IV]. This behavior is different from what happens in other zinc-blende-derived monolayer superstructures where these deep valence bands interact strongly.[25]

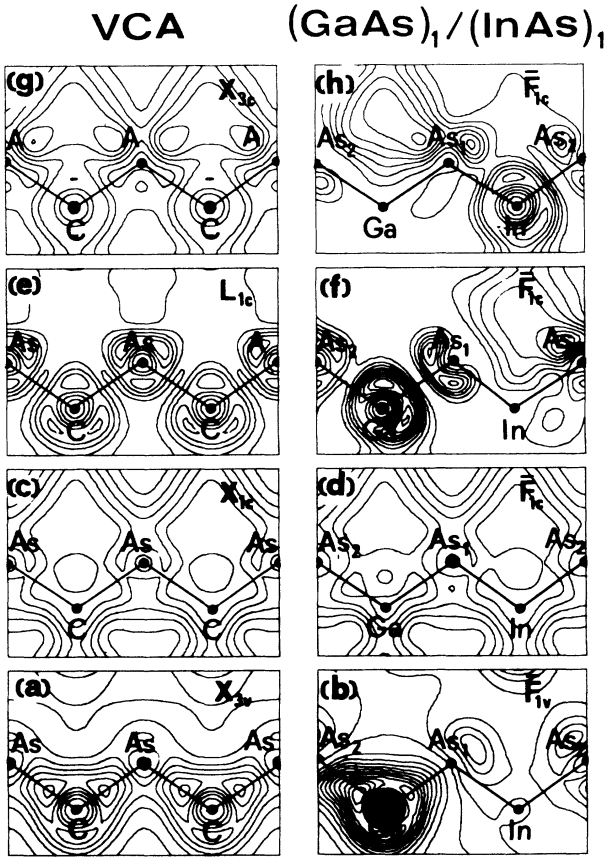

FIG. 6. The same as Fig. 4 for valence- and conduction-band states at the $\bar{F}$ point. The step between two neighboring contours is 1.

On the other hand, the change in the electronic charge distribution is dramatic for the higher valence and conduction bands. The highest valence states as the Γ_{15v}, X_{5v}, and L_{3v} states (Fig. 4), with a prevalent anionic p character, combine and split due to the system symmetry reduction in a nondegenerate component with charge-density lobes along the [111] direction and in another state, doubly degenerate in the case of the Γ_{15v} state, with the charge maxima onto the orthogonal plane. Notice that the energy splitting is small and these states do not shift substantially with respect to the corresponding virtual-crystal states. Since they do not interact substantially with other valence states or with the first conduction states, the global change in their orbital character should be negligible. Indeed, recent LAPW calculations performed on similar systems give evidence of a very small s- and d-orbital mixing in the Γ_{15v}-derived states.[32]

The intermediate valence states strongly interact with each other. As a consequence of the interaction, electronic charge is transferred onto a given layer. Consider, for example, the two $\bar{F}_{1v}$ (X_{3v}) [Fig. 6(b)] and $\bar{F}_{1v}$ (L_{1v}) [Fig. 5(c)] states. The energy splitting between the virtual-crystal X_{3v} and L_{1v} states is approximately 0.04 eV (see Table III). In the superlattice these two states turn out to belong to the same irreducible representation.

The strong interaction splits the charge density: in the $\bar{F}_{1v}$ (X_{3v}) state it piles up on the Ga—As(2) bond, while in the $\bar{F}_{1v}$ (L_{1v}) state it does so on the In-As(1) one. The state-energy split is 0.233 eV.

As far as the conduction states are concerned, we can see from the charge-density plots that a substantial charge rearrangement takes place on passing from the virtual crystal to the superlattice. The virtual-crystal Γ_{1c} and L_{1c} states [Figs. 5(e) and 5(f)], which are mapped by the folding operation into the same superlattice $\bar{\Gamma}$ point, interact, giving rise to two $\bar{\Gamma}_{1c}$-symmetry states strongly localized in the two different layers: the lower-energy state on the Ga-As(2) layer, the higher-energy one on the In-As(1) one. The energy split is remarkable, as already mentioned.

Another interaction example, symmetric to the valence one given above, concerns the two virtual-crystal L_{1c} and X_{3c} states [Figs. 6(e)–6(h)]. The energy order in the virtual crystal is X_{1c}, L_{1c}, and X_{3c}, X_{1c} being the lowest-energy state. In fact, its energy is lower than that of the L_{1c} state in the compressed InAs. Unlike the Γ_{1c} and L_{1c} states, the X_{1c} states lower their energy with the uniform compression in both binary constituents. The virtual-crystal L_{1c} and X_{3c} states give rise to two $\bar{F}_{1c}$ states in the superlattice. An inspection of the charge-density redistribution reveals the lowest conduction state in $\bar{F}$ is a binary L_{1c} and X_{3c} mixed state. The charge-density distribution associated with the $\bar{F}_{1c}$ (X_{1c}) state [Fig. 6(d)] is not considerably modified, showing a relatively weak interaction with other states. A strong interaction takes place, on the other hand, between the two L_{1c} and X_{3c} states, with a considerable splitting in the charge-density distribution. The energy splitting is such that the X_{3c}-state energy increases by about 0.17 eV, while the L_{1c}-state one diminishes by about 0.265 eV. As a consequence, an inversion in the energy order between the two binary L_{1c}- and X_{1c}-derived states occurs.

Referring to these strongly coupled states with the nomenclature appropriate to the ZB symmetry states is only a matter of convenience. Indeed, as it can be seen from the charge-density plots associated with these states their symmetry properties are totally changed and they no longer have any resemblance to their parent states in the binary compounds.

2. *Superlattice orientation effect*

We do not intend to carry out a systematic study of the differences in the band structures of different oriented superlattices; rather our purpose is simply to show that the strength of the electronic state interactions and the possible consequent charge localizations, as we found in the (111) monolayer superlattice, are closely related to the particular superlattice orientation. A recent theoretical study has indeed detailed the dependence of the minimum band gap and of the related bowing coefficient on the particular superlattice orientation.[32]

Consider the first conduction state in the superlattice $\bar{\Gamma}$ point. The strong electronic charge localization on the Ga-As(2) layer [and the corresponding localization on the In-As(1) layer of the second conduction state] in a monolayer superlattice is quite surprising. First-principles calculations of electronic states in (001)-oriented ultrathin superlattices have provided evidence of charge confinement,[13,27,28] even if the localization does not occur in the thinner (001) monolayer or bilayer superlattices. However, the possibility of charge localization in atomically thin superlattices has been predicted.[28] In our case it is a consequence of a particular strong coupling between the electronic states.

In the (111) monolayer superlattice this effect is closely related to the geometry of the system. In order to give evidence of this, we performed a comparison with the [001]-oriented monolayer superlattice. In Fig. 7 the planar average of the electronic charge distribution associated to the first $\bar{\Gamma}_{1c}$ state and of the self-consistent potential (the local part) is plotted along the superlattice direction for both systems. The averaged electronic charge density is larger in the GaAs layer also in the (001) system, even if it does not give rise to any localization. This different behavior can be qualitatively interpreted considering the superlattice formed by ultrathin quantum wells whose shape and width are related to the potential behavior. The wells and barriers turn out to be more definite for the (111)- than for the (001)-oriented superlattice. The localization of the first conduction state in the GaAs layer can be explained by considering the calculated minimum band gaps in the Γ Point in the two endpoint materials at the same superlattice lattice constant, 0.627 eV in GaAs and 1.276 eV in InAs, and a rough estimation of the valence-band offset for the Ga-In-As system,[42,43] that

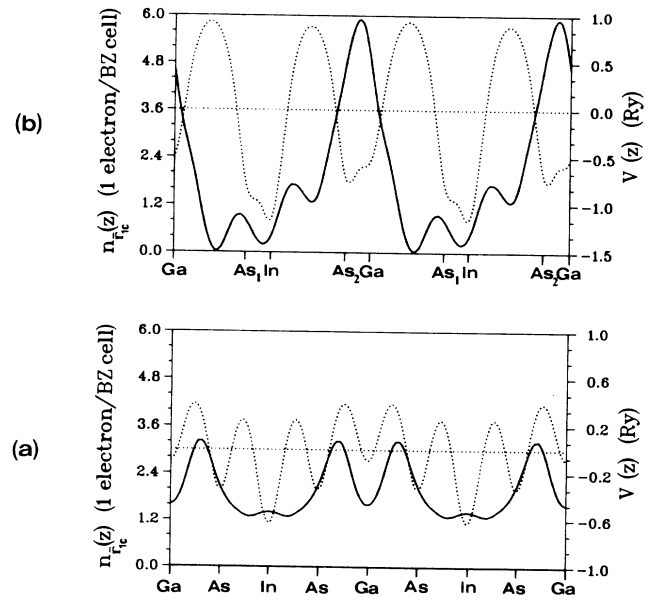

FIG. 7. Planar average of the self-consistent local potential (dashed curve) and of the first conduction state electronic charge density (solid curve) plotted along the superlattice direction for the unrelaxed (a) [001]- and (b) [111]-oriented $(GaAs)_1/(InAs)_1$ superlattices.

gives it very near to zero. This estimation is also consistent with the charge delocalization in the valence-band-edge state found in the present calculation [Fig. 4(f)]. Therefore, the quantum wells occur in the GaAs layer for electrons.

To explain the different behavior between the two different oriented superlattices, it is necessary to take into account, besides the Γ_{1c} offsets, also the offset of the conduction states that are strongly coupled with them in the superlattices: the L_{1c} states in the (111) superlattices and the X_{1c} states in the (001) superlattices. The L_{1c} offset turns out to be about 0.65 eV, while the X_{1c} offset is much less, about 0.21 eV. The quantum wells for the first two conduction states are deeper for the (111) than for the (001) superlattices. The strong coupling between the electronic states in the III-V compound superlattices makes the charge-localization description somewhat different from the one appropriate, for instance, for the Si/Ge superlattices.[27,28]

We stress that the arguments used here are only qualitative, since it is well known that the valence-band offset depends closely on the superlattice thickness,[13] on the strain condition,[28,29,44] and, to a lesser extent, on its orientation.[15,45]

Moreover, the charge localization is made possible by the unequivalency of the two arsenic atoms in the unit cell of the (111) monolayer superlattice, which allows for a different charge distribution around them. In the (001) superlattice the two arsenic atoms cannot be distinct.

Related to the strength of the interaction between the first and the second conduction state in $\bar{\Gamma}$ is the different value of the minimum band gap we obtained for the two different oriented superlattices in their unrelaxed configuration. Our calculated values are 0.701 eV for the (111) superlattice and 0.836 eV for the (001) superlattice.

In order to compare the minimum band gaps for systems of different symmetry, we calculated their values for the two binary systems by using different unit cells [the primitive cell, the doubled trigonal and tetragonal unit cells appropriate, respectively, to the (111) and (001) monolayer superlattices] and different **k** points for the BZ integrations performed in order to obtain the self-consistent potential. For the (111) trigonal unit cell we used two special **k** points, while for the (001) tetragonal unit cell we used the two nonspecial **k** points proposed by Bernard and Zunger.[25] We found a difference between the calculated minimum band gaps of 0.028 eV for GaAs and of 0.075 eV for InAs, the smaller values being in both cases those appropriate to the tetragonal symmetry. Therefore, the 0.14-eV difference between the calculated band gaps of the two different oriented superlattices turns out to be significative of a pure orientation effect. This result is in agreement with the 200-meV reduction of the direct band gap taking place on passing from the (001) to the (111) configuration in the lattice-matched $GaAlAs_2$ system, obtained by Wei *et al.*,[32] who used a self-consistent LAPW method and corrected their LDA values for the discrepancy with the experimental values.[32] On the basis of the results given by the same authors in the case of the $GaInP_2$ system, which has a lattice mismatch similar to the $GaInAs_2$ one, we do not expect that the inclusion of the structural relaxation, important in these systems, may change substantially this situation.

C. From the unrelaxed to the relaxed (111) superlattice

Because of the large lattice mismatch between the two binary constituents, the unrelaxed geometry is not the equilibrium configuration. To obtain a lower-energy configuration we allowed the (111) planes to shift along the longitudinal direction. The assumed relaxation model is described in detail in Ref. 19. The relaxed configuration preserves the space group of the undistorted superlattice. The lattice constant perpendicular to the superlattice direction has been kept fixed to the unrelaxed superlattice equilibrium value, while the parallel dimension has been allowed to change. Moreover, we assumed only two distinct nearest-neighbor (NN) bond distances d_{GaAs} and d_{InAs}. The minimum-energy configuration has been achieved with the unit cell dilated vertically 1.4% and equilibrium bond distances $d_{GaAs}=2.434$ Å and $d_{InAs}=2.491$ Å.

From Table III, where the calculated eigenvalues, relative to the valence-band maximum (VBM), are given, we notice that the structural relaxation introduces new relevant features in the superlattice band structure. The electronic states already split on passing from the virtual crystal to the unrelaxed superlattice by the introduction of the chemical disparity of the two cations undergo further changes in their energies, due to the introduction of the different NN bond distances and of the vertical dilation of the unit cell. The states derived from the ZB Γ_{15v} and Γ_{15c} states show an apparently curious behavior. While the two $\bar{\Gamma}_{3v}$ and $\bar{\Gamma}_{1v}$ states split a further 210 meV and reverse their energy order, the two $\bar{\Gamma}_{3c}$ and $\bar{\Gamma}_{1c}$ states diminish their splitting with respect to the unrelaxed case and do not give rise to any energy inversion.

To explain these changes in the band structure, we rely upon the fact that the superlattice in this relaxed configuration can be thought to originate from the alternate superimposition of layers of trigonally distorted GaAs and InAs. In these layers the dimension parallel to the (111) planes is taken equal to the superlattice one, while the layer height is adjusted to give Ga—As and In—As bond distances equal, respectively, to the equilibrium ones in the superlattice relaxed configuration. So, the changes and the splittings occurring in the relaxed superlattice band structure can be understood by analyzing the effects of the trigonal distortion on the band energies in the two binary compounds when they are subjected to a compressive or tensile lateral strain on the (111) planes. Also, this procedure permits us to compare the effects related to the introduction of the two distinct cations (step B earlier) with those related to the epitaxial strain. Both these transformations give rise to the passage of the system from the cubic to a trigonal symmetry. The epitaxial strain, whose amount is measured by the η parameter defined in Ref. 19, which gives the ratio between the actual height of the unit cell c and the ideal one, $c_0=a/\sqrt{3}$, alters the zinc-blende BZ in a way similar to the folding. The relation between the superlattice $\bar{\Gamma}$ and $\bar{F}$ points and the parent L and X points in the binary compounds is not as direct as in the unrelaxed case. In this case the folding

does not map exactly the original zinc-blende points onto $\bar{\Gamma}$ and $\bar{F}$, where $\bar{F}$ are still the points at the center of the BZ rectangular faces. We can consider the folded states in these points as originating from binary L' and X' states somewhat strain altered and whose point groups are those appropriate to the trigonal symmetry (see Tables I and II).[46]

In Fig. 8 we depict the variation in the Γ-point electronic state energies that takes place on passing from the undistorted [Figs. 8(a) and 8(e)] to the trigonally distorted binaries [Figs. 8(b) and 8(d)] and finally to the relaxed superlattice [Fig. 8(c)]. The original undistorted binary L states are given for reference. In the case of GaAs, whose unit cell turns out to be compressed along the [111] direction by about 2%, we observed the following features.

(1) The Γ_{15v} state, triply degenerate in the cubic configuration, splits to form the doubly-degenerate Γ_{3v} and the nondegenerate Γ_{1v} states. The doubly-degenerate state energy is lower, namely 265 meV. This energy splitting has to be compared with the corresponding one occurring in the unrelaxed superlattice and related to the difference between the two cation pseudopotentials, which is only 6 meV.

(2) A similar splitting also occurs for the Γ_{15c} state.

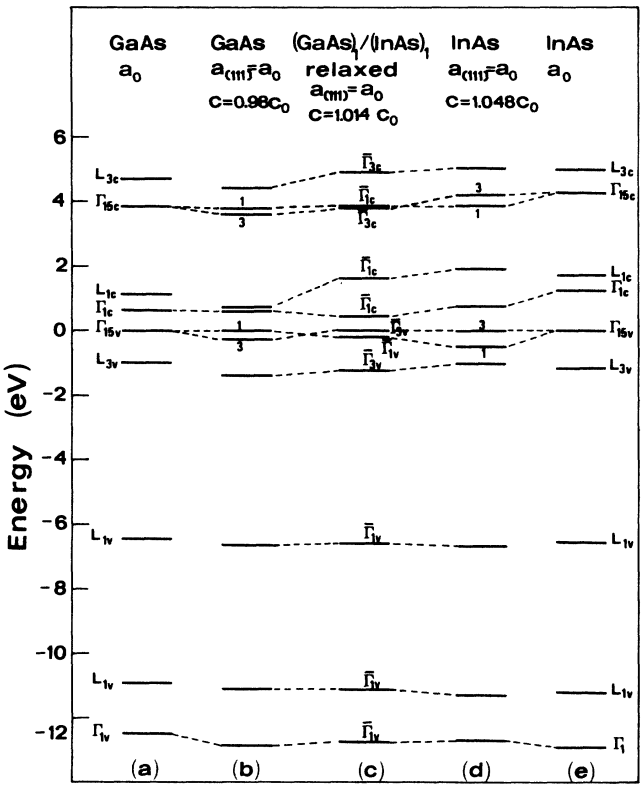

FIG. 8. Band eigenvalues at the Brillouin-zone center for (a) and (e) cubic GaAs and InAs at the lattice constant $a_0=5.66$ Å, (b) and (d) trigonally distorted GaAs and InAs whose lattice parameter along the [111] direction is $a=c\sqrt{3}\neq a_0$, and (c) relaxed $(GaAs)_1/(InAs)_1$ (111) superlattice. The binary systems have been folded back into the half-volume Brillouin zone appropriate to a double unit cell.

The energy difference between the two split states is slightly smaller than for the corresponding valence states. This gives evidence of another difference between the strain and the new crystal-ordering-induced potentials: while the latter has a much larger effect on the conduction than on the valence states (see Fig. 3), the former does not make a substantial distinction between them.

(3) Another relevant variation concerns the two Γ_{1c} and L'_{1c} states that approach each other considerably, mostly because of the lowering (0.354 eV) of the L'_{1c} state. The minimum band gap in the trigonally distorted GaAs does not change substantially. In fact, it diminishes by only 19 meV. An inspection of the electronic charge distributions of these two states shows that the strain induces only a distortion in the charge contours, whose relevance is directly related to the strain strength itself. The charge localization in given crystal layers that takes place in the two first conduction states of the superlattice is to be attributed only to the superlattice ordering potential effects.

As far as the InAs is concerned, we can observe that the reversal of the strain (the InAs layers turn out to be dilated by about 4.7% along the [111] direction) gives rise to an inversion of the Γ_{15} split states with respect to the GaAs case. Now the nondegenerate states have a lower energy than the doubly-degenerate ones. The splitting strength is higher (0.528 eV between the Γ_{1v} and Γ_{3v} states and 0.396 eV between the Γ_{1c} and Γ_{3c} ones), and is approximately related to the strain strength. The unit-cell dilation, differently from the compression, gives rise to a further energy splitting between the Γ_{1c} and L'_{1c} states and, in this case, the Γ_{1c} state lowers its energy considerably. As a consequence the minimum band gap in the trigonally distorted InAs is reduced from 1.276 to 0.756 eV.

In light of the results obtained on the two binary systems it is easy to understand the changes that take place in the superlattice state energies on passing from the unrelaxed to the relaxed configuration. The energy inversion between the $\bar{\Gamma}_{3v}$ and $\bar{\Gamma}_{1v}$ states at the valence-band top is due to the larger weight of dilated InAs in the relaxed superlattice configuration. From Fig. 8 we can see that the relaxed superlattice states are almost midway between the corresponding ones of the two trigonally distorted parent binary compounds with minor differences to be attributed to the ordering potential effect; that is, to the charge transfers occurring between the compressed and dilated layers. These charge transfers are not exactly equal to those occurring in the unrelaxed case and this can be seen, for instance, by comparing Fig. 8 with Fig. 2, where the unrelaxed superlattice bands are given together with the bands of the undistorted binaries. Particular attention has been devoted to the first two $\bar{\Gamma}_{1c}$ conduction states that split further by 0.222 eV. The splitting is to be attributed entirely to the lowering of the first $\bar{\Gamma}_{1c}$ state that dramatically reduces the minimum band gap. From the comparison between Figs. 2 and 8 we notice that, unlike the undistorted situation, the corresponding Γ_{1c} states in the two distorted parent binary compounds are almost at the same energy. The interaction between them is stronger and shifts the $\bar{\Gamma}_{1c}$ state down in the relaxed

configuration.

We observed in the discussion on the effects of the new ordering potential that an interaction between band states takes place in correspondence with any relevant energy splitting. In this case, the imposition of the epitaxial strain on the superlattice gives rise to a further splitting between the first two conduction states, but it does not substantially affect their coupling. This can be understood, in the second-order perturbation-theory scheme, by observing that the energy difference between the average energies of the Γ_{1c} and L_{1c} states in the two binary systems increases slightly with the strain by about 0.18 eV, reducing the coupling between the corresponding states in the superlattice. As a consequence, the charge localization in the first conduction state in the $\bar{\Gamma}$ point turns out to be reduced, as can be noticed by looking at Fig. 9. In this figure the planar-average charge-density distribution of the first $\bar{\Gamma}_{1c}$ state is plotted along the [111] direction both for the unrelaxed and relaxed superlattices. In the schematic representation of the superlattice by ultrathin quantum wells, the relaxation produces a small change in the width of wells and barriers. Indeed there is no substantial modification in the shape of the planar-average self-consistent-field local potential. Moreover, the estimated two minimum band gaps in the distorted parent binary compounds building up the relaxed superlattice are much closer than in the unrelaxed situation (0.608 eV in GaAs and 0.756 eV in InAs) with a lowering of their offset by about 0.5 eV, while the L_{1c} offset increases by about the same amount. Moreover, an inspection to the valence-band-edge–state charge distribution reveals a relevant piling up of charge in the InAs(1) layer (Fig. 10). The epitaxial strain, giving rise to the Γ_{15v} level splitting at the VBM in the two parent binary compounds, should have changed the valence-band offset with respect to the undistorted situation in such a way that the depths of the wells in the GaAs(2) layer for electrons are not substantially affected, as can be deduced by the almost negligible charge reduction in the GaAs layer (Fig. 9).

Finally, the calculated total band-gap–bowing parameter for this ordered structure is defined as[11]

$$b_{\mathrm{ord}}(\bar{\Gamma}_{1c})=4[\bar{\varepsilon}(\Gamma_{1c})-\varepsilon(\bar{\Gamma}_{1c}(\Gamma_{1c}))] ,$$

where $\bar{\varepsilon}(\Gamma_{1c})$ is the average value of the direct band gaps in the two binary compounds at their equilibrium volumes. We obtained $b_{\mathrm{ord}}(\bar{\Gamma}_{1c})=2.69$ eV for the $(GaAs)_1/(InAs)_1$ (111) superlattice.

The contributions to the bowing parameter coming from the three distinct conceptual steps [volume deformation (VD), chemical exchange (CE), and structural relaxation (S)], in which we imagine the superlattice has been formed, are defined as[25,32]

$$b_{\mathrm{VD}}(\Gamma_{1c})=2[\varepsilon_{\mathrm{GaAs},a_{\mathrm{eq}}^{\mathrm{GaAs}}}(\Gamma_{1c})+\varepsilon_{\mathrm{InAs},a_{\mathrm{eq}}^{\mathrm{InAs}}}(\Gamma_{1c})] -2[\varepsilon_{\mathrm{GaAs},a_0}(\Gamma_{1c})+\varepsilon_{\mathrm{InAs},a_0}(\Gamma_{1c})] ,$$

where a_0 is the intermediate equilibrium lattice constant of the superlattice in its unrelaxed configuration,[19]

$$b_{\mathrm{CE}}(\bar{\Gamma}_{1c}(\Gamma_{1c}))=2[\varepsilon_{\mathrm{GaAs},a_0}(\Gamma_{1c})+\varepsilon_{\mathrm{InAs},a_0}(\Gamma_{1c})] -4\varepsilon_{\mathrm{unrelaxed}}(\bar{\Gamma}_{1c}(\Gamma_{1c})) ,$$

where $\varepsilon_{\mathrm{unrelaxed}}(\bar{\Gamma}_{1c}(\Gamma_{1c}))$ is the direct band gap of the (111) superlattice in its unrelaxed configuration, and finally

$$b_S(\bar{\Gamma}_{1c}(\Gamma_{1c}))=4[\varepsilon_{\mathrm{unrelaxed}}(\bar{\Gamma}_{1c}(\Gamma_{1c}))-\varepsilon(\bar{\Gamma}_{1c}(\Gamma_{1c}))] .$$

In the present calculation $b_{\mathrm{VD}}=0.71$ eV, $b_{\mathrm{CE}}=1.00$ eV, and $b_S=0.98$ eV for the $GaInAs_2$ (111) superlattice.

The bowing coefficients b for the VCA disordered alloy band eigenvalues are defined in a similar manner:[11]

$$b_{\mathrm{VCA}}=4(\bar{\varepsilon}-\varepsilon_{\mathrm{VCA}}) ,$$

where $\bar{\varepsilon}$ is the average-band eigenvalue of the parent binary compounds. For the Γ_{1c} state we obtained $b_{\mathrm{VCA}}=0.29$ eV.

The reported experimental band-gap–bowing parame-

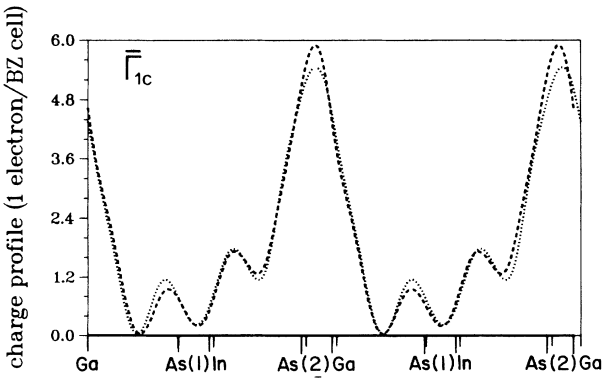

FIG. 9. Planar average of the first conduction state electronic charge density for the unrelaxed (dashed curve) and the relaxed (dotted curve) configuration plotted along the superlattice direction. The atomic plane positions before (the longest tic marks) and after relaxation are shown.

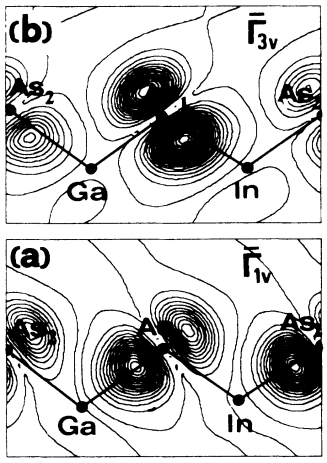

FIG. 10. Charge density of the superlattice valence-band-edge state (a) before and (b) after the relaxation plotted as in Fig. 4.

ters for $Ga_xIn_{1-x}As$ disordered alloys are 0.33–0.56 eV (Ref. 47) and 0.61 eV.[48]

Our results confirm the outcomes of other recent calculations[12,25,32] that the superlattice ordering leads to an increase of the band-gap–bowing parameter, while the VCA treatment of the disordered alloy underestimates it with respect to the experimental values. Moreover, our results compare well with those recently obtained by Wei *et al.*[32] They find for the $GaInP_2$ system in the same crystal structure a total band-bowing coefficient $b_{ord}=1.82$ eV, with the volume-deformation contribution $b_{VD}=0.66$ eV and the chemical-exchange one $b_{CE}=0.82$ eV, while the structural relaxation contributes with $b_S=0.34$ eV. For the lattice-matched $GaAlAs_2$ system they have $b_{CE}=1.45$ eV. By considering the different computational approach used here, the b_{VD} value we obtained for the $GaInAs_2$ system, which has a lattice mismatch similar to the $GaInP_2$ one, and the b_{CE} value, which scales correctly with the electronegativity difference with respect to the $GaAlAs_2$ system, are in reasonable agreement. The larger value obtained here for b_S is due to the different relaxation model, which in our case also includes a dilation of the unit cell, besides moving the internal freedom degrees.[19] Thus, we find that the uniaxial strain of the unit cell has a large effect on the direct band gap and therefore on the band-bowing parameter related to it.

IV. CONCLUSIONS

We have presented a first-principles calculation of the electronic band structure of $(GaAs)_1/(InAs)_1$ (111) superlattice. We found considerable modifications in the electronic charge distributions at the high-symmetry points, arising mainly for two reasons: (a) the symmetry reduction of the system, which displays a preferred direction instead of the zinc-blende cubic isotropy, and (b) the interaction between some folded states mapped onto the same **k** point in the new Brillouin zone and belonging to the same irreducible representation. The superlattice noninteracting states show charge-density distributions similar to those displayed by the corresponding states in the trigonal strained parent binary compounds. In the interacting states, on the other hand, the imposition of the new long-range order introduces new features, as a considerable piling up of charge on a given sublattice. Among them, the first two conduction states at the Brillouin-zone center turn out to be strongly localized on the Ga-As(2) (the lower-energy state) and In-As(1) layers. Moreover, the fundamental band gap is considerably reduced. A comparison with the unrelaxed $GaInAs_2$(001) monolayer superlattice reveals that this charge localization and the minimum band gap depend on the superlattice orientation. The fundamental band gap is smaller for the (111) orientation. The structural relaxation of the superlattice giving rise to a slight unit-cell dilation further reduces the minimum band gap, increasing the corresponding band-bowing parameter. The energy splitting of the triply-degenerate Γ_{15} states due to the trigonal distortion of the unit cell is considerably larger than those related to the new superlattice ordering potential. The relaxation reduces the charge localization in the first conduction state and leads to a charge localization on the In-As(1) layer in the VBM state.

ACKNOWLEDGMENTS

The author wishes to thank Professor C. Calandra for his encouragement and for a critical reading of the manuscript. The calculations have been carried out at the Computational Center of the University of Modena [Centro Interdipartimentale di Calcolo Automatico e Informatica Applicata (CICAIA)], whose technical assistance and support is acknowledged. This work was supported by Consiglio Nazionale delle Ricerche (CNR) and Ministero della Pubblica Istruzione, Italy.

[1]T. S. Kuan, T. F. Kuech, W. I. Wang, and E. L. Wilkie, Phys. Rev. Lett. **54**, 201 (1985).
[2]H. Nakayama and H. Fujita, in *GaAs and Related Compounds, 1985,* IOP Conf. Ser. No. 79, edited by M. Fujimoto (Hilger, London, 1986).
[3]H. R. Jen, M. J. Cherng, and G. B. Stringfellow, Appl. Phys. Lett. **48**, 1603 (1986).
[4]T. S. Kuan, W. I. Wang, and E. L. Wilkie, Appl. Phys. Lett. **51**, 51 (1987).
[5]T. Fukui and H. Saito, Jpn. J. Appl. Phys. **23**, L521 (1984).
[6]T. Fukui, H. Saito, and Y. Tokura, Jpn. J. Appl. Phys. **27**, L1320 (1988).
[7]T. Wada and Y. Maeda, Appl. Phys. Lett. **53**, 1596 (1988).
[8]Y. E. Ihm, N. Otuska, J. Klem, and H. Morkoç, Appl. Phys. Lett. **51**, 2013 (1987).
[9]M. A. Shahid, S. Mahajan, D. E. Laughlin, and H. M. Cox, Phys. Rev. Lett. **58**, 2567 (1987); M. A. Shahid and S. Mahajan, Phys. Rev. B **38**, 1344 (1988).
[10]A. Gomyo, T. Suzuki, and S. Iijima, Phys. Rev. Lett. **60**, 2645 (1988).
[11]D. M. Wood, S.-H. Wei, and A. Zunger, Phys. Rev. B **37**, 1342 (1988).
[12]P. Boguslawski and A. Baldereschi, in *Excitons in Confined Systems,* edited by R. Del Sole, A. D'Andrea, and A. Lapiccirella (Springer-Verlag, Berlin, 1988), pp. 151–158.
[13]S. Ciraci and I. P. Batra, Phys. Rev. Lett. **58**, 2114 (1987).
[14]A. Oshiyama and M. Saito, Phys. Rev. B **36**, 6156 (1987).
[15]D. M. Bylander and L. Kleinman, Phys. Rev. B **36**, 3229 (1987); **38**, 7480 (1988).
[16]J. E. Bernard, L. G. Ferreira, S.-H. Wei, and A. Zunger, Phys. Rev. B **38**, 6338 (1988).
[17]S.-H. Wei and A. Zunger, Phys. Rev. Lett. **61**, 1505 (1988).
[18]T. Ohno, Phys. Rev. B **38**, 13 191 (1988).
[19]R. Magri and C. Calandra, Phys. Rev. B **40**, 3896 (1989).
[20]A. A. Mbaye, D. M. Wood, and A. Zunger, Phys. Rev. B **37**, 3008 (1988); A. A. Mbaye, A. Zunger and D. M. Wood, Appl. Phys. Lett. **49**, 782 (1986).
[21]J. L. Martins and A. Zunger, Phys. Rev. Lett. **56**, 1400 (1986).

[22]D. M. Wood and A. Zunger, Phys. Rev. Lett. **61**, 1501 (1988).
[23]C. P. Flynn, Phys. Rev. Lett. **57**, 599 (1986).
[24]R. Magri and C. Calandra, Superlatt. Microstruct. **5**, 1 (1989).
[25]J. E. Bernard and A. Zunger, Phys. Rev. B **36**, 3199 (1987).
[26]A. Taguchi and T. Ohno, Phys. Rev. B **36**, 1696 (1987); **38**, 2038 (1988).
[27]M. S. Hybersten and M. Schlüter, Phys. Rev. B **36**, 9683 (1987).
[28]S. Froyen, D. M. Wood, and A. Zunger, Phys. Rev. B **37**, 6893 (1988).
[29]C. G. Van de Walle and R. M. Martin, Phys. Rev. B **34**, 5621 (1986).
[30]T. Kurimoto, N. Hamada, and A. Oshiyama, Superlatt. Microstruct. **5**, 171 (1989).
[31]S.-H. Wei and A. Zunger, Appl. Phys. Lett. **53**, 2077 (1988).
[32]S.-H. Wei and A. Zunger, Phys. Rev. B **39**, 3279 (1989).
[33]J. P. Perdew and M. Levy, Phys. Rev. Lett. **51**, 1884 (1983).
[34]R. W. Godby, M. Schlüter, and L. J. Sham, Phys. Rev. Lett. **56**, 2415 (1986).
[35]C. Mailhiot and D. L. Smith, Phys. Rev. B **35**, 1242 (1987); **38**, 5520 (1988).
[36]C. J. Bradley and A. P. Cracknell, *The Mathematical Theory of Symmetry in Solids* (Clarendon, Oxford, 1972).
[37]D. R. Hamann, M. Schlüter, and C. Chiang, Phys. Rev. Lett. **43**, 1494 (1979); G. B. Bachelet, D. R. Hamann, and M. Schlüter, Phys. Rev. B **26**, 4199 (1982).
[38]D. M. Ceperley and B. J. Alder, Phys. Rev. Lett. **45**, 566 (1980).
[39]J. P. Perdew and A. Zunger, Phys. Rev. B **23**, 5048 (1981).
[40]G. P. Srivastava, J. L. Martins, and A. Zunger, Phys. Rev. B **31**, 2561 (1985).
[41]M. Kondow, S. Minagawa, Y. Inoue, T. Nishino, and Y. Hamakawa, Appl. Phys. Lett. **54**, 1760 (1989).
[42]A. D. Katnani and G. Margaritondo, J. Appl. Phys. **54**, 2522 (1983).
[43]M. Cardona and N. E. Christensen, Phys. Rev. B **37**, 1011 (1988).
[44]D. Gershoni, H. Temkin, J. M. Vandenberg, S. N. G. Chu, R. A. Hamm, and M. B. Panish, Phys. Rev. Lett. **60**, 448 (1988).
[45]A. Baldereschi, S. Baroni, and R. Resta, Phys. Rev. Lett. **61**, 734 (1988).
[46]R. Magri (unpublished).
[47]J. Hwang, P. Pianetta, Y.-C. Pao, C. K. Shih, Z.-X. Shen, P. A. P. Lindberg, and R. Chow, Phys. Rev. Lett. **61**, 877 (1988).
[48]D. Von Bimberg, R. Blachnik, M. Cardona, P. J. Dean, T. Grave, G. Harbeke, K. Hübner, U. Kaufmann, W. Kress, O. Madelung, W. von Munch, U. Rössler, J. Schneider, M. Schulz, and M. S. Skolnick, in *Physics of Group IV Elements and III-V Compounds,* Vol. 17a of *Landolt-Börnstein,* edited by O. Madelung (Springer-Verlag, Berlin, 1982).